Physica 24D (1987) 279–291
North-Holland, Amsterdam

LORENZ-LIKE CHAOS IN A PARTIAL DIFFERENTIAL EQUATION FOR A HEATED FLUID LOOP*

James A. YORKE[1], Ellen D. YORKE[2] and John MALLET-PARET[3]

Received 22 January 1986
Revised manuscript received 23 May 1986

A set of partial differential equations are developed describing fluid flow and temperature variation in a thermosyphon with particularly simple external heating. Several exact mathematical results indicate that a Bessel–Fourier expansion should converge rapidly to a solution. Numerical solutions for the time-dependent coefficients of that expansion exhibit a transition to chaos like that shown by the Lorenz equations over a wide range of fluid material parameters.

1. Introduction

The Lorenz equations [1] are one of the earliest examples of the occurrence of chaos in differential equations arising in a physically interesting model. The equations

$$\dot{x} = -\sigma(x-y),$$
$$\dot{y} = -xz - rx - y,$$
$$\dot{z} = xy - bz,$$

were obtained by a severe truncation of a double Fourier expansion of the equations for fluid convection between two horizontal parallel plates.

For the parameters ($\sigma = 10$, $b = \frac{8}{3}$) first used by Lorenz, they predict a well-defined route to chaos as the Rayleigh number, r, is increased from zero. We summarize this below. For $r < 1$, the steady state $(0,0,0)$ is stable. This point corresponds to the fluid at rest with a linear vertical temperature profile, hot at the bottom and cool on top. At $r = 1$, this state becomes unstable and steady convective circulation represented by the fixed points $(\pm b\sqrt{r-1}, \pm b\sqrt{r-1}, r-1)$ (clockwise or counterclockwise flow) becomes stable. These two fixed points remain stable for $r < r_H = \sigma(\sigma+b+3)/(\sigma-b-1)$. At $r = r_H$, a subcritical Hopf bifurcation occurs and for $r > r_H$ chaotic time dependence of the velocity and temperature are predicted as shown in fig. 1a. The shape of Lorenz's chaotic attractor for r not too much larger than r_H is quite distinctive. Its projection onto the xz plane is shown in fig. 1b. For $r_c < r < r_H$, chaotic and steady motions coexist with the fate of the system depending upon whether initial conditions lie in the basin of attraction of the Lorenz attractor or of one of the fixed points. At r_c a crisis occurs [2, 3] and the strange attractor is destroyed, though for a range of $r < r_c$, transient chaos [4] is observed. For $\sigma = 10$, $b = \frac{8}{3}$, $r_c \approx 24.06$ and $r_H = 24.74$, but the same route to chaos has been observed for other values of σ and b with the transitional Rayleigh numbers altered accordingly. For high values of r and in some ranges of b and σ other types of behavior (periodic orbits, period doubling, and asymmetric periodic and chaotic

*This research was partially supported by grants from the National Science Foundation (DMS 84-19110 and MES 79-05774-05) and the Air Force Office of Scientific Research (AFOSR-81-0217).

[1]University of Maryland, College Park, MD 20742, Institute for Physical Science and Technology and Department of Mathematics, USA.

[2]University of Maryland Baltimore County, Catonsville, MD 21228, Department of Physics, USA.

[3]Brown University, Providence, RI 02912, Center for Applied Mathematics, USA.

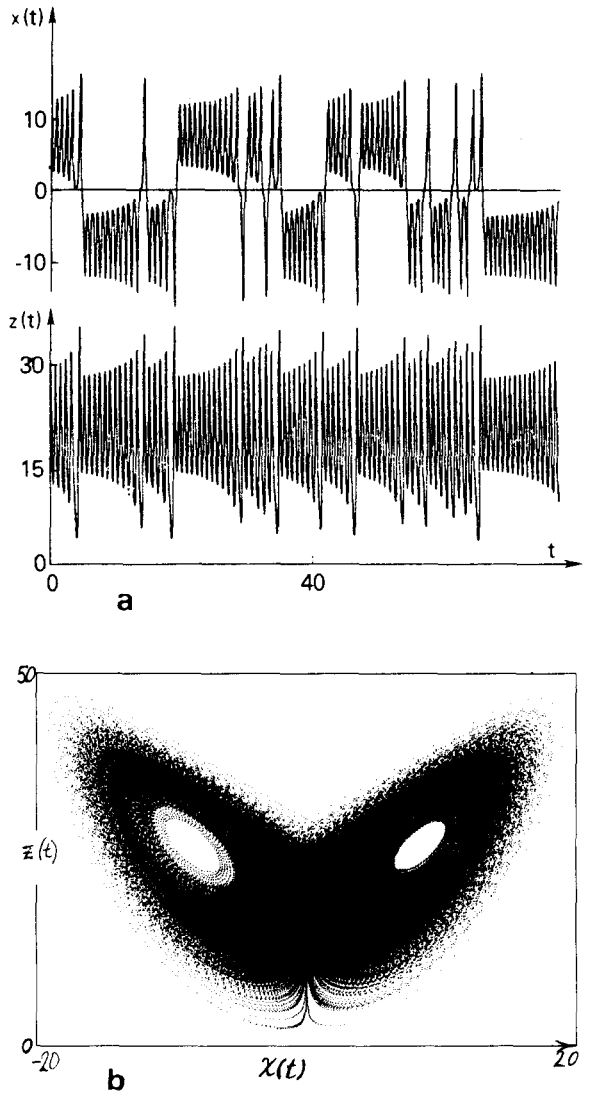

Fig. 1. a) A sample solution of Lorenz's system with $b = \frac{8}{3}$, $\sigma = 10$, $r = 28$; b) The projection of a solution onto the xz plane.

trajectories) have all been observed and are described in an extensive review by Sparrow [5].

The Rayleigh–Bénard convection geometry which originally motivated the Lorenz equations does not follow the route to chaos just described because the three-dimensional nature of that geometry – ignored in the truncation – plays a crucial role in the transition to time dependent motion. However, it has been suggested that the Lorenz equations might better describe convective flow in a closed circular pipe called a natural circulation loop or thermosyphon which is heated from below and cooled from above, as shown in fig. 2. Welander [6] observed chaotic oscillations in a numerical simulation of a thermosyphon and Creveling [7] observed irregular oscillations experimentally in a closed fluid loop. More recently, Gorman et al. [8] have experimentally observed the Lorenz scenario for transition to chaos in such a system. There is a large literature on thermosyphons. They have engineering applications in solar heating and cooling systems and some passive cooling methods for nuclear reactors. (For a survey, see Mertol and Greif [9].)

Our objective is to describe the transition to chaos in a partial differential equation representing a simple thermosyphon. The heating and cooling mechanism is assumed to be particularly simple and the fluid velocity is zero at the walls of the tube. Because the resulting equations are still too complex to solve numerically with sufficient accuracy to reliably predict the behavior of realistic solutions, we make one further restriction. We require the fluid velocity to be aligned along the tube so that each point of the fluid remains a constant distance from the wall of the tube and we further assume that the instantaneous velocity depends only on the distance from the center of the tube (as would be the case if the tube was straight). Accepting these restrictions the resulting system of equations can be studied theoretically and numerically with considerable precision and the transitions to and from chaos can be identified. Our partial differential equation does predict transitions which are qualitatively similar to those of the Lorenz equations although they occur at larger values of the Rayleigh numbers r_H and r_c.

2. The equations and the approximation of the solutions

We consider an incompressible fluid whose density depends upon temperature as

$$d = d_0(1 + \delta(T_0 - T)).$$

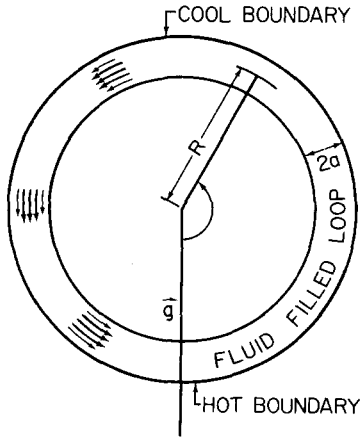

Fig. 2. A thermosyphon, heated from below, cooled from above.

The fluid's thermal conductivity will be denoted χ, its viscosity ν, and its thermal expansion coefficient δ, and it fills a toroidal tube of cross section radius a and height $2R$. The tube is oriented vertically in a uniform gravitational field with strength g. Angular distance φ around the tube is measured counterclockwise from direction of gravity as shown in fig. 2 and radial coordinate ρ is measured from the center of the tube of the wall ($0 \le \rho \le a$). The quantities χ, ν, δ and d_0 are assumed to be temperature independent.

We examine the case in which the walls of the tube are maintained at a time-independent temperature $T_W(\varphi)$ that depends only on the angle φ and that this establishes the temperature of the fluid at the wall. Specifically we assume the wall temperature is given by

$$T_W(\varphi) - T_0 = W\cos\varphi, \tag{1}$$

where T_0 is the temperature at the "equator" of the tube. We assume good thermal contact between the fluid and the wall so the fluid's temperature at the wall equals the wall temperature.

There is considerable experimental work on thermosyphons, though often the heating at the bottom is via a constant heat flux; that is, the tube is wrapped in wires that generate heat at a constant rate. The top of the tube may be enclosed in a cooling jacket. Nonetheless our boundary conditions do represent a realistic physical experiment that was suggested by A. Faller [personal communication] but, as far as we know, has not been performed. He proposed hollowing out a loop from a block of aluminum as a conduit for the fluid. Heating the aluminum at the bottom and cooling it on top would produce a linear temperature gradient in the aluminum. As measured by φ, eq. (1) would be satisfied, except for minor corrections due to the thickness of the tube. It is our hope that our findings might be of assistance in locating and describing chaotic transitions in experiments of such a design.

The fluid is described by the Navier–Stokes equation

$$\frac{\partial \boldsymbol{v}}{\partial t} + (\boldsymbol{v}\cdot\nabla)\boldsymbol{v} = -\frac{1}{d_0}\nabla P + (1+\delta(T_0 - T))\boldsymbol{g} + \nu\nabla^2\boldsymbol{v} \tag{2a}$$

and the heat equation

$$\frac{\partial T}{\partial t} + \boldsymbol{v}\cdot\nabla T = \chi\nabla^2 T. \tag{2b}$$

The previously mentioned restrictions imply that $\boldsymbol{v} = v(\tau, t)\hat{\varphi}$ where $\hat{\varphi}$ is the unit vector along the tube and $T = T(\rho, \varphi, t)$ while the boundary conditions require that

$$v(a, t) = 0 \tag{2c}$$

and

$$T(a, t, \varphi) = T_W(\varphi). \tag{2d}$$

For a narrow tube, the rate of change of temperature across the tube is generally much more rapid than along the tube, so we will ignore diffusion along the tube. We therefore replace ∇^2 – which includes $(1/R^2)\partial^2/\partial\varphi^2$ – with $\nabla_\rho^2 = (1/\rho)(\partial/\partial\rho)(\rho\partial/\partial\rho)$ which includes only the terms across the tube. The pressure P is eliminated by integrating (2a) around a circular path at fixed ρ; this, together with the restriction on v reduces

(2a) to

$$\frac{\partial v}{\partial t} = \nu \nabla_\rho^2 v + \frac{\delta g}{2\pi} \int_0^{2\pi} T \sin\varphi \, d\varphi, \tag{3a}$$

while (2b) may be rewritten

$$\frac{\partial T}{\partial t} + \frac{v}{R} \frac{\partial T}{\partial \varphi} = \chi \nabla_\rho^2 T. \tag{3b}$$

We will now describe the regularity properties of the solution in order to assure that the solutions can be found numerically. Specifically we expand the difference between the solution temperature $T(\rho, \varphi, t)$ and the wall temperature in a Fourier series in φ so the coefficients C_k and S_k depend on ρ and t, that is,

$$T(\rho, \varphi, t) = T_W(\varphi) + \sum_k \big(C_k(\rho, t) \cos(k\varphi) + S_k(\rho, t) \sin(k\varphi) \big). \tag{4}$$

Generally we will simply write C and S when k is 1. Our theoretical findings can be described as follows.

A) The partial differential equations for $v(\rho, t)$, $C(\rho, t)$, and $S(\rho, t)$ decouple from C_k and S_k for $k > 1$, so it is possible to determine v, S, and C without reference to the higher frequency terms of the Fourier series.

B) $\int_0^a (C_k^2(\rho, t) + S_k^2(\rho, t)) \rho \, d\rho \to 0$ as $t \to \infty$ for each $k > 1$.

C) The functions $C(\rho, t)$, $S(\rho, t)$, and $v(\rho, t)$ are bounded for all time.

The following assertion is a folk theorem which appears to be unpublished. While experts have assured us it is valid, we have seen no proof.

D) The functions $v(\rho, t)$, $C(\rho, t)$ and $S(\rho, t)$ are infinitely differentiable. Furthermore v, C and S and their partial derivatives of all orders taken with respect to ρ and t are uniformly bounded for all time.

E) When C and S are expanded in Bessel functions in ρ, the nth coefficients (functions of time) go to 0 as $n \to \infty$ and in fact they go to 0 like $n^{-5/2}$. These coefficients satisfy ordinary differential equations involving all the other Bessel function coefficients (but not their derivatives) so truncating the system after a finite number of Bessel terms has little effect on the solutions.

In particular we may expect to represent the solutions accurately using only a small number of Bessel function coefficients. Of course when the solutions are chaotic, they will be sensitive to initial data, but we may expect solutions of the truncated system to *statistically* represent the real solutions. That is, the transitions to chaos will occur at about the same parameter values. We now proceed to argue for properties A through E.

Properties A and B. Using the notation of (4) and multiplying both sides of (3b) by $\sin(k\varphi)$ or $\cos(k\varphi)$ and integrating, we obtain

$$\frac{\partial v}{\partial t} = \nu \nabla_\rho^2 v + \frac{\delta g S}{2} \tag{5}$$

while for $k \neq 1$

$$\begin{aligned} \frac{\partial S_k}{\partial t} &= \frac{k}{R} v C_k(\rho, t) + \chi \nabla_\rho^2 S_k, \\ \frac{\partial C_k}{\partial t} &= \frac{-k}{R} v S_k(\rho, t) + \chi \nabla_\rho^2 C_k, \end{aligned} \tag{6}$$

and for $k = 1$

$$\begin{aligned} \frac{\partial S}{\partial t} &= vC/R + \chi \nabla_\rho^2 S - vW/R, \\ \frac{\partial C}{\partial t} &= -vS/R + \chi \nabla_\rho^2 C. \end{aligned} \tag{7}$$

As asserted in (A) above, the equations (5, 7) for v, S and C are independent of S_k and C_k for $k > 1$. Notice further (using (6)) that for $k > 1$

$$\frac{1}{2} \frac{\partial}{\partial t} \big(S_k^2 + C_k^2 \big) = \chi \big(S_k \nabla_\rho^2 S_k + C_k \nabla_\rho^2 C_k \big).$$

Integrating over the cross section area of the tube,

$$\frac{\partial}{\partial t}\int_0^a (S_k^2 + C_k^2)\rho\,d\rho\,\alpha$$
$$\times \int_0^a \frac{1}{\rho}\left\{ S_k \frac{\partial}{\partial \rho}\rho\frac{\partial S_k}{\partial_\rho}\right) + C_k \frac{\partial}{\partial_\rho}\rho\frac{\partial C_k}{\partial \rho}\right)\Big\}\rho\,d\rho$$
$$= \int_0^a \frac{\partial}{\partial_\rho}\left(S_k\rho\frac{\partial S_k}{\partial \rho} + C_k\rho\frac{\partial S_k}{\partial \rho}\right)$$
$$-\rho\left[\left(\frac{\partial C_k}{\partial \rho}\right)^2 + \left(\frac{\partial C_k}{\partial \rho}\right)^2\right]d\rho.$$

Since $S_k = C_k = 0$ at $\rho = a$, the first term vanishes. Then

$$\frac{1}{2}\frac{\partial}{\partial t}\int_0^a (S_k^2 + C_k^2)\rho\,d\rho$$
$$= -\int_0^a \rho\left[\left(\frac{\partial S_k}{\partial \rho}\right)^2 + \left(\frac{\partial C_k}{\partial \rho}\right)^2\right]d\rho < 0,$$

implying that these modes with $k \neq 1$ die out with time, establishing *B*.

Property C: boundedness of C, S and v. Since heat diffuses and is carried by convection and is generated nowhere in the interior, it is not surprising that the temperature remains unbounded, and if everywhere in the loop the temperature initially is between $-W$ and W (the extremes of the wall temperature), it must stay between $-W$ and W for all time. We will now be more precise in establishing a bound on T for all time.

Imagine a temperature distribution $U_1 = \alpha(a - \rho^2) + \beta$ with $\alpha > 0$ and $\beta > W$. Whatever the actual temperature distribution $T(\rho, \varphi, 0)$ is at time 0, we choose α and β so that

$$U_1(\rho) - T(\rho, \varphi, 0) > 0$$
for all φ and $\rho, 0 \le \rho \le a$.

We claim

$$U_1(\rho) > T(\rho, \varphi, t) \tag{8}$$

for all (ρ, φ, t) and in particular since the maximum of U_1 is $\alpha a + \beta$, it follows that this is a bound for all time. Suppose (8) were not true for all time. Then there would be a first time t_0 for which it fails. At t_0 the difference $U_1 - T$ drops to 0 somewhere though it is positive elsewhere: that is,

$$U_1(\rho) - T(\rho, \varphi, t_0) \ge 0 \quad \text{for all } \rho, \varphi$$

and $T(\rho_0, \varphi_0, t_0) = U_1(\rho_0)$ for some ρ_0, φ_0. Since $U_1 - T$ has a minimum in the tube at ρ_0, φ_0 when $t = t_0$ and since U_1 does not depend on φ then if we fix ρ and vary φ, T has a maximum. Therefore we must have

$$T_\varphi = \frac{\partial}{\partial \varphi} T(\rho_0, \varphi_0, t_0) = 0.$$

In addition, the point ρ_0, φ_0, t_0 is a minimum of $U_1 - T$ if we vary only ρ so

$$\nabla_\rho^2 U_1(\rho) - \nabla_\rho^2 T \ge 0 \quad \text{so} \quad -\nabla_\rho^2 T \ge 4\alpha.$$

In addition (3b) yields

$$\frac{\partial}{\partial t}\left[U_1(\rho_0) - T(\rho_0, \varphi_0, t_0)\right]$$
$$= vT_{\varphi/R} - \chi\nabla_\rho^2 T \ge 0 - \chi\nabla_\rho^2 U_1$$
$$= 4\chi\alpha > 0.$$

Thus our assumptions imply $U_1 - T_1$ is increasing at (ρ_0, φ_0) but (ρ_0, φ_0, t_0) is the first point at which $U_1 - T$ has *dropped* to 0. Therefore we have a contradiction and no such t_0 exists. Hence $U_1 > T$ for all time. Notice if we choose the special form $T = S\sin\varphi + C\cos\varphi$ and letting S, C, and v satisfy (5–7), then T is a solution so S and C are bounded for all time. By symmetry T and S and C are also bounded from below.

We now show $v(t, \rho)$ is bounded. By the previous argument $S(t, \rho)$ is less than some value $S_{\max}$ for all time. Choose

$$U_2(\rho) = \alpha(a - \rho^2) + \beta$$

so that $\alpha > \frac{1}{4}\delta g S_{\max}/\nu$ and $\beta > 0$ and

$$U_2(\rho) - v(0, \rho) > 0 \quad \text{for all } 0 \le \rho \le a.$$

We claim

$$U_2(\rho) - v(t, \rho) > 0 \tag{9}$$

for all t and $0 \le \rho \le a$. In particular, it follows that v is bounded for all time by $\alpha a + \beta$. Suppose (9) were not true. Then there would be a first time t_0 for which it fails. At t_0, $U_2 - v$ drops to 0 somewhere while it is positive elsewhere. Hence for some ρ_0, t_0, we have $U_2(\rho_0) - v(t_0, \rho_0) = 0$. However, at such a point

$$\nabla_\rho^2[U_2 - v] > 0 \quad \text{and} \quad -\nabla_\rho^2 v > 4\alpha,$$

and

$$\frac{\partial}{\partial t}[U_2(\rho_0) - v(t_0, \rho_0)] = -\nabla_\rho^2 v - \tfrac{1}{2}\delta g S$$
$$> 4\alpha\nu - \tfrac{1}{2}\delta g S_{\max} > 0.$$

Thus our assumptions imply $U_2 - v$ would be strictly increasing at the point. But ρ_0, t_0 is the first point at which $U_2 - v$ has dropped to 0. So no such t_0 exists. Hence $U_2 > v$ for all time. By symmetry, $v(t, \rho)$ is also bounded from below.

Property D: differentiability of solutions. Eqs. (5)–(7) are independent of φ so we write ∇_ρ^2 simply as ∇^2, the Laplacian with respect to x in the plane. Writing $u(t, x) = (v(t, x), S(t, x), C(t, x))$ for x in the plane, $|x| \le a$, eqs. (5, 7) may be written

$$\frac{\partial u}{\partial t} = M\nabla^2 u + g(u), \tag{10}$$

where M is the diagonal matrix having diagonal entries ν, χ, χ. The function g is

$$g(v, S, C) = \left(\frac{\delta g}{2} S, \frac{1}{R} vC + \frac{1}{R} vW, -\frac{1}{R} vS\right). \tag{11}$$

The smoothness of solutions is claimed to follow from the following attributes:

i) the function g is infinitely differentiable in all variables and does not depend on any of the partial derivatives of u;

ii) the region (denoted D – a disk) is bounded and has a smooth boundary (denoted ∂D);

iii) $u = 0$ on the boundary and the initial state $u(0, x)$ is infinitely differentiable with respect to x (as we may assume);

iv) it must be known that $|u|$ is bounded for all $t \ge 0$ (as established above).

Under these conditions it is asserted by the folk theorem that for all integers $\alpha \ge 0$ and $\beta \ge 0$

$$\left|\frac{\partial^{\alpha+\beta} u(t, x)}{\partial t^\alpha \partial x^\beta}\right| \quad \text{is bounded for all } t \ge 0 \text{ and for all } x \text{ in } D.$$

The bound depends on α and β. In fact we require this for $\alpha + \beta$ up to 6.

Property E. Let ψ_k be the eigenfunction of ∇_ρ^2 with eigenvalue λ_k, i.e., ψ_k is a Bessel function of order zero satisfying

$$\lambda_k \psi_k = \nabla_\rho^2 \psi_k \quad \text{where } \psi_k = 0 \text{ on the boundary } \partial D. \tag{12}$$

The eigenfunctions are normalized, i.e., $\int_D \psi_k^2 = 1$. As in the discussion of property D we confine the argument to functions of ρ alone so $\nabla_\rho^2 = \nabla^2$. We recall that for any functions ψ and u

$$\int_D u\nabla^2\psi = \int_{\partial D} u\frac{\partial \psi}{\partial n} - \int_D \nabla u \cdot \nabla\psi$$
$$= \int_{\partial D}\left(u\frac{\partial \psi}{\partial n} - \frac{\partial u}{\partial n}\psi\right) + \int_D (\nabla^2 u)\psi, \tag{13}$$

where $\partial/\partial n$ is the normal derivative on the boundary. If u is expanded in functions ψ_k, the

expansion coefficients U_k satisfy

$$U_k = \int_D u\varphi_k = \frac{1}{\lambda_k}\int_D u\nabla^2\psi_k$$

$$= \frac{1}{\lambda_k}\int_{\partial D}\left(u\frac{\partial\psi}{\partial n} - \frac{\partial u}{\partial n}\psi_k\right) + \frac{1}{\lambda_k}\int_D(\nabla^2 u)\psi_k.$$

We are interested in the case where u is one of the components of the vector $\bar{u}$ – that is, u is either v, C or S. Therefore the ∂D integral is 0 since the first term has a factor u and the second ψ_k both of which vanish on ∂D. Repeating the process twice yields

$$U_k = \frac{1}{\lambda_k^2}\int_D \nabla_u^2\nabla^2\psi_k$$

$$= \frac{1}{\lambda_k^2}\left[\int_{\partial D}\nabla^2 u\frac{\partial\psi_k}{\partial n} - \frac{\partial}{\partial n}\nabla^2 u\psi_k\right]$$

(#1) (#2)

$$+\frac{1}{\lambda_k^2}\int_D(\nabla^2)^2 u\psi_k$$

(#3)

and term #3 is given by

$$(\#3) = \frac{1}{\lambda_k^3}\left[\int_{\partial D}(\nabla^2)^2 u\frac{\partial\psi_k}{\partial n} - \frac{\partial}{\partial n}(\nabla^2)^2 u\psi_k\right]$$

(#4) (#5)

$$+\frac{1}{\lambda_k^3}\int(\nabla^2)^3 u\psi_k.$$

(#6)

Terms #2 and #5 are 0 since ψ_k is 0 on ∂D.

In term #1 we note that $u = 0$ on ∂D so $\partial u/\partial t = 0$ so

$$0 = \frac{\partial}{\partial t}u = M\nabla^2 u + g(u).$$

Thus $\nabla^2 u = -M^{-1}g(0)$ since $u = 0$ on the boundary. Also $g(0) = 0$ so $\nabla^2 u = 0$ on the boundary, so term #1 is 0. To evaluate #6 we use the Schwartz inequality

$$|\#6| \le \frac{1}{\lambda_k^3}\left\{\int_D\left[(\nabla^2)^3 u\right]^2\right\}^{1/2}\left\{\int_D\psi_k^2\right\}^{1/2}.$$

the $\int\psi_k^2$ term is 1 and the folk theorem says the partial derivatives making up $(\nabla^2)^3 u$ are all bounded so that the integral is bounded (and independent of k) and we obtain

$$|\#6| \le 0\left(\frac{1}{\lambda_k^3}\right).$$

Term (#5) is not as nice. Indeed $(\nabla^2)^2 u$ is bounded but $\partial\psi/\partial n$ is not, and in our case of Bessel functions $\partial\psi/\partial n - \lambda_k^{1/2}$, yielding a $\lambda_k^{-5/2}$ term, which is also a $k^{-5/2}$ term. Hence

$$|U_k| \approx k^{-5/2}.$$

This conclusion suggests the coefficients are decaying rapidly and can be ignored for moderately large k. We note that on the boundary $(\nabla^2)^2 u$ is indeed generally non-zero and can be evaluated by taking ∇^2 of both sides of (10). Since $\nabla^2 u = 0$ on the boundary, so is $\partial/\partial t\nabla^2 u$. Hence

$$(\nabla^2)^2 u = -M\nabla^2 g(u).$$

This has non-zero terms $\nabla v\cdot\nabla C$ and $\nabla v\cdot\nabla S$ which are non-zero on the boundary.

Coupled ordinary differential equations. The boundary conditions (2c) and (2d) make it appropriate to expand v, C and S in a series of Bessel functions of order zero, $J_0(\alpha_N\rho/a)$, where α_N is the nth zero of the Bessel function. The time-dependent coefficient of $J_0(\alpha_N\rho/a)$ are $v_N(t)$, $c_N(t)$ and $s_N(t)$ and they satisfy the following infinite set of coupled differential equations:

$$\dot{v}_N = -\nu\left(\frac{\alpha_N}{a}\right)^2 v_N + \frac{\delta g}{2}s_N,$$

$$\dot{s}_N = \frac{1}{R}\sum_{nm}\gamma_{Nnm}v_n c_m - \chi\left(\frac{\alpha_N}{a}\right)^2 s_N + \frac{W}{R}v_N,$$

$$\dot{c}_N = -\frac{1}{R}\sum_{nm}\gamma_{Nnm}v_n s_m - \chi\left(\frac{\alpha_N}{a}\right)^2 c_N,$$

with

$$\gamma_{Nnm} = \int_0^1 J_0(\alpha_N x) J_0(\alpha_n x) J_0(\alpha_m x) x \, dx / \left(J_1^2(\alpha_N)/2\right).$$

The connection between these equations and the Lorenz equations can be made particularly clear by measuring time, t, in terms of the dimensionless quantity

$$\tau = \frac{\chi \alpha_1^2}{a^2} t$$

and using other dimensionless quantities as defined below:

$$r = \frac{\delta g}{2\chi\nu}\left(\frac{a}{\alpha_1}\right)^4 \frac{W}{R},$$

$$\sigma = \nu/\chi,$$

$$G_{Nnm} = 2^{3/2} \int_0^1 J_0(\alpha_N x) J_0(\alpha_m x) J_0(\alpha_n x) x \, dx / |J_1(\alpha_N) J_1(\alpha_n) J_1(\alpha_m)|,$$

$$X_N = \frac{a^2}{R_\chi} \frac{|J_1(\alpha_N)|}{\sqrt{2}} \frac{v_N}{A_N};$$

$$A_N = 1 \text{ if } N \neq 1; \quad A_1 = \frac{\alpha_1^2}{G_{111}},$$

$$Y_N = \frac{\delta g a^4 |J_1(\alpha_N)|}{2^{3/2} R \chi \nu} \frac{s_N}{B_N};$$

$$B_N = 1 \text{ if } N \neq 1; \quad B_1 = \alpha_1^2 A_1,$$

$$Z_N = \frac{-\delta g a^4 |J_1(\alpha_N)|}{2^{3/2} R \chi \nu} \frac{c_N}{B_N},$$

$$H_{Nnm} = G_{Nnm}/\alpha_1^2; \quad n, m \neq 1;$$

$$H_{N1m} = \frac{G_{N1m}}{G_{111}}; \quad H_{Nm1} = \frac{\alpha_1^2 G_{N1m}}{G_{111}};$$

$$H_{N11} = \alpha_1^4 \frac{G_{N11}}{G_{111}}.$$

In terms of these variables (with $\dot{x} = dx/d\tau$, etc.) we find

$$\dot{X}_1 = -\sigma(X_1 - Y_1),$$

$$\dot{Y}_1 = -Y_1 + rX_1 - X_1 Z_1 - \sum_{n=2}^{\infty} G_{11n}\left(X_1 Z_n/\alpha_1^4 + x_n z_1/\alpha_1^2\right) - \sum_{m=2}^{\infty}\sum_{n=2}^{\infty} G_{111} G_{1nm} X_m Z_n/\alpha_1^6,$$

$$\dot{Z}_1 = -Z_1 + X_1 Y_1 + \sum_{2}^{\infty} G_{11n}\left(X_1 Y_n/\alpha_1^4 + X_n Y_1/\alpha_1^2\right) + \sum_{2}^{\infty}\sum_{2}^{\infty} G_{111} G_{1nm} X_n Y_m/\alpha_1^6$$

and for $N \neq 1$

$$\dot{X}_N = -\left(\sigma/\alpha_1^2\right)\left(\alpha_N^2 X_N - Y_N\right),$$

$$\dot{Y}_N = -\frac{\alpha_N^2}{\alpha_1^2} Y_N + \alpha_1 r X_N - H_{N11} X_1 Z_1 - \sum_{m,n\neq 1} H_{Nmn} X_m Z_n - \sum_{m\neq 1} \left(H_{N1m} X_1 Z_m + H_{Nm1} X_m Z_1\right),$$

$$\dot{Z}_N = -\frac{\alpha_N^2}{\alpha_1^2} Z_N + H_{N11} X_1 Y_1 + \sum_{n,m\neq 1} H_{Nmn} X_m Y_m + \sum_{m\neq 1} \left(H_{N1m} X_1 Y_m + H_{Nm1} X_m Y_1\right).$$

The above system of equations for X, Y, and Z will collectively be denoted (*) and the same notation will be used for the truncated system. As in the original Lorenz equations σ is the Prandtl number of the fluid ($\sigma = \nu/\chi$) and r is proportional to the impressed temperature gradient W/R.

We truncate the system at N modes by setting X_i, Y_i, Z_i identically zero for all time for $i > N$. The N mode system has $3N$ equations. When we truncate to one mode the equations reduce to the Lorenz equations with $b = 1$. We have numerically

explored the effect of truncating the equations at various values of N and we discuss that in the next section. Numerically convergence seems to be good.

3. Results

We have studied truncations of eqs. (*) involving up to five radial modes for a range of values of σ in the region $r < 100$. The stability of the origin can be investigated by linearizing eqs. (*) around $(0,0,0)$. Modes of different index N then decouple and the first positive eigenvalue appears at $r = 1$ with successive positive eigenvalues appearing at $r = \alpha_N^4/\alpha_1^3$. Thus flow in this model commences at the same value $r = 1$ as for the Lorenz equations.

For $r > 1$ we solved the $3N$ equations resulting from a truncation to N modes on an IBM PC using a fourth order Runge-Kutta method. The step size used ranged from 0.01 to 0.001 and was set to achieve a compromise between small error and reasonable run time. In general the changes in the value of any one of the variables upon making a single step was at least 10^4 time greater than the estimated error per step in that variable.

The route to chaos we observed is similar to that for the Lorenz system in the same parameter range. For low values of $r > 1$ there are two nonzero steady states which, numerically, are stable under small perturbations. The symmetry of eqs. (*) requires that these two steady states be at points of the form (X_*, Y_*, Z_*) and $(-X_*, -Y_*, Z_*)$. The numerical values of (X_1, Y_1, Z_1) at the steady state for $N > 1$ differ by 10% or less from the prediction $(\pm\sqrt{r-1}, \pm\sqrt{r-1}, r-1)$ for the Lorenz system $(N = 1)$ with $b = 1$. The Hopf bifurcation value, r_H, can be accurately found by observing whether an orbit close to the fixed point spirals in or out. The dependence of r_H on σ and N is summarized in fig. 3. The Lorenz equations predict $r_H = \sigma(\sigma + 4)/(\sigma - 2)$, a curve with a broad minimum at

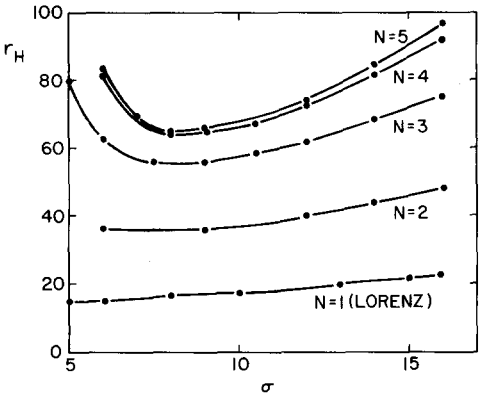

Fig. 3. Hopf bifurcation values r_H plotted as a function of σ.

$\sigma \approx 5.46$ which rises to infinity at $\sigma = 2$ and increases linearly with σ at large σ. As the number of radial modes is increased, r_H increases for all σ. The change in r_H resulting from the addition of

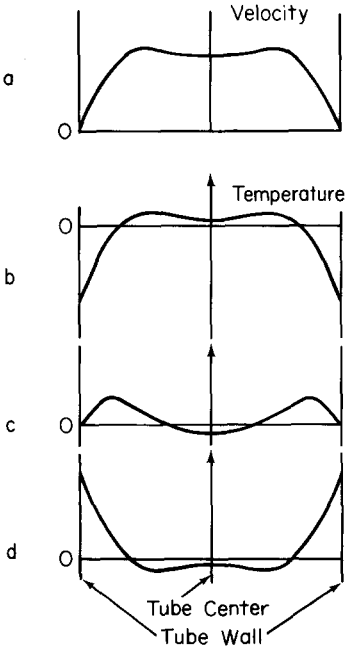

Fig. 4. a) The steady state velocity profile across the tube. The velocity is zero on the boundary and does not peak at the center. The temperature of the steady state is shown in b) measured at the top of the tube; in c) at midheight, $\phi = \pi/2$, as the fluid is moving downward; and in d) at the bottom.

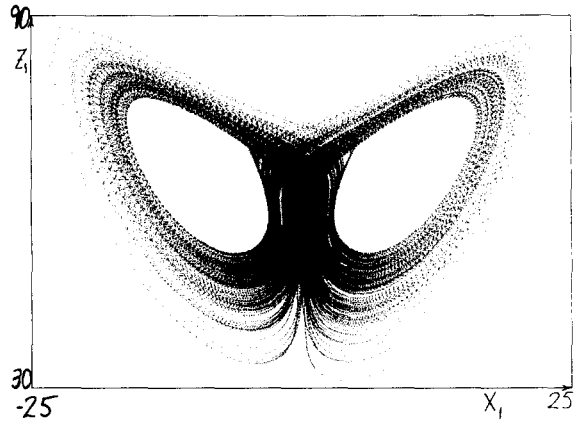

Fig. 5. For the $N = 5$ mode system $X_1(t)$ is plotted against $Z_1(t)$ with time step 0.005, $r = 60.0$, $\sigma = 10.0$.

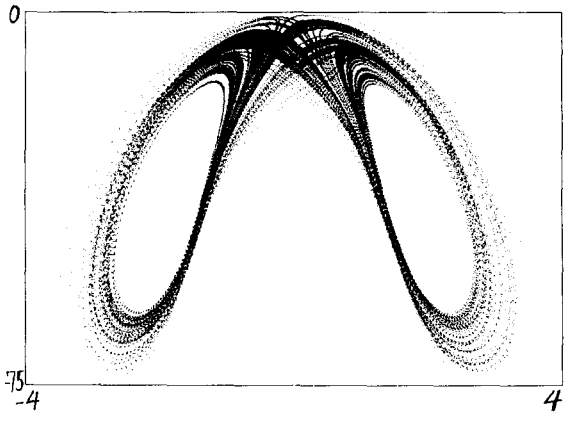

Fig. 6. The parameters used are the same as in fig. 5. The velocity of a solution is averaged across the tube at each time and is plotted horizontally against the temperature (vertical axis) averaged across the tube at $\varphi = 0$, the bottom.

extra radial modes becomes less severe as N is increased, with $N = 4$ and $N = 5$ giving quite similar results (in line with our expectations that the truncation will converge). For low σ, r_H increases more rapidly then for the Lorenz system (for $N = 5$, r_H exceeds 100 at $\sigma = 5$). The minimum is sharpened and shifted to higher Prantdl number ($\sigma \approx 9$ for $N = 5$) and the slope of r_H vs. σ for higher σ is about five times larger than for the three dimensional system. These results suggest that the steady state will become unstable at a thermal gradient which is approximately four times greater than that predicted by the single mode truncation for the same size tube for a Prandtl number like that of room temperature water ($\approx$ 6.5) and the discrepency would be even worse for very viscous or highly heat conducting fluids.

The steady state flow profile and the temperature profile at different locations around the tube can easily be obtained and are plotted in figs. 4a and 4b–d for a steady state five-mode system. The shapes of these profiles depend only on r (σ does not enter into the equations at steady state). The fluid velocity and temperature are fairly constant over the interior of the tube; most variation occurs for $\rho > 0.6a$.

Above r_H, chaotic flow is observed for the multimode system which is qualitatively similar to the flow seen in the Lorenz system. Fig. 5 is a plot of Z_1 vs. X_1 in the chaotic regime with $N = 5$. The similarity to fig. 1b is striking. The velocity and temperature at the bottom of the tube under conditions of chaotic flow averaged over the cross section of the tube – that is

$$\int_0^a v(\rho, t)\rho \, d\rho \quad \text{and}$$

$$\int_0^a (T(\rho, \varphi = 0, t) - W)\rho \, d\rho$$

is shown in fig. 6 for the same parameter values as used in 5 and these more physical quantities also occupy a region very similar in shape to the Lorenz system's attractor.

Lorenz discovered that the dynamics of the Lorenz equations could be described by a numerically generated quasi one-dimensional map. From the numerical solution of the differential equations he recorded successive peaks $z_1, z_2, \ldots$ of the coordinate z. The plot of z_{n+1} vs. z_n lies along a cusped curve as shown in fig. 7a to a precision of within 1 part in 10^3 (which is masked on the scale of the graph). We have plotted a similar peak map for successive maxima of Z_1 for $N = 5$. Despite the large number of modes involved, the peak map shows strong resemblence to the Lorenz system maps. Although it is slightly thicker – less "one-

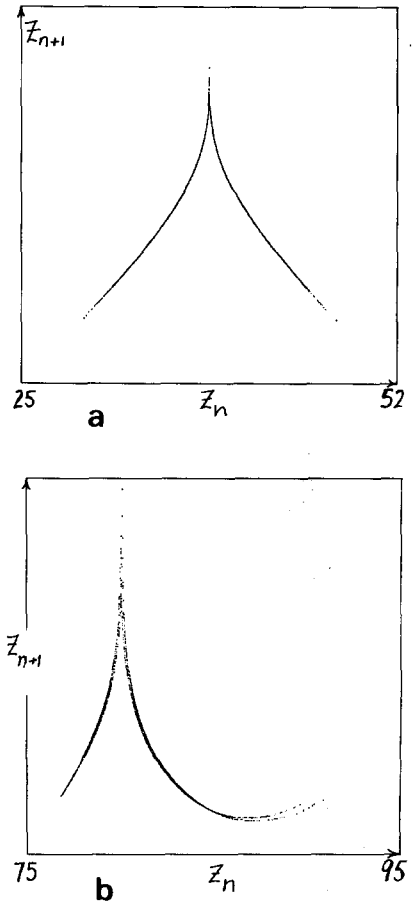

Fig. 7. The successive maxima Z_n of the $Z_1(t)$ are obtained numerically and are plotted horizontally against Z_{n+1}. In (a) we use the standard Lorenz system with 8500 pairs plotted. In (b) we use $N = 4$ modes, $\sigma = 10$, $\rho = 60$, plotting 2700 pairs.

dimensional" – its closeness to a single curve indicates the dominance of an attracting region of phase space of dimension not much higher than two.

As r is decreased below r_H, a chaotic attractor and attracting steady state solutions are observed to coexist for a range of values of r, as in the Lorenz system. (In reality we cannot distinguish between chaos and long-transient transient chaos.) A lower bound on the crisis value, r_c, is located by starting slightly above r_H, gradually reducing r and allowing the system to run for 250 time units before reducing r again. An orbit is called transient if it begins to decay to the steady state within this time. The results are shown in fig. 8. Again we notice the general trend that the additional modes drive transitions to higher values of r (relative to the $N = 1$ truncation) and again the results for $N = 4$ and $N = 5$ are close, encouraging our belief that the truncation is converging. The interval, $r_c < r < r_H$, is much broader (for any given σ) for the multimode systems than for $N = 1$. For $\sigma > 14$ we do not find the same sort of crisis as at lower σ, but rather some complex behavior including one-sided periodic and one-sided chaotic orbits in a wedge shaped region of parameter space marked "one-sided" in fig. 8. Below the wedge, the only attractors are stationary solutions. As r is increased a one-sided periodic orbit arises in a saddle-node bifurcation. It undergoes a period doubling sequence to one sided chaos as r is increased further. As r is increased further, leaving the wedge, the chaotic attractor is destroyed in a crisis at the high r edge of its region of existence in parameter space. An example of one-sided chaos and its associated peak map is shown in fig. 9. In this case the motion of the fluid is predominantly in one direction. When such an orbit is seen, the

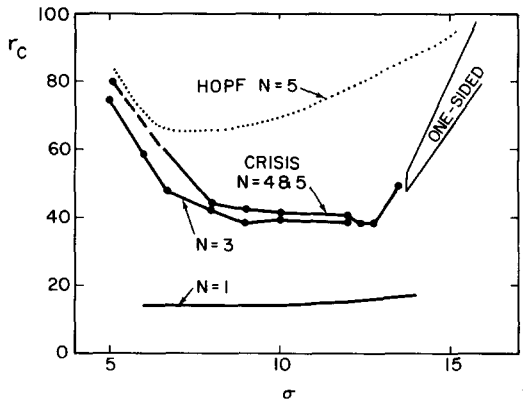

Fig. 8. The numerically estimated crisis values r_c are shown for $N = 1$, 3, and 4–5 modes. The cases for 4 and 5 cannot be distinguished and are plotted as a single curve. Below these crisis curves no sustained chaos is seen. Above the curve we see sustained chaos (for at least 200 oscillations of the solution studied). For $N = 5$ the stable steady state coexists with chaos up to r_H, the dotted curve.

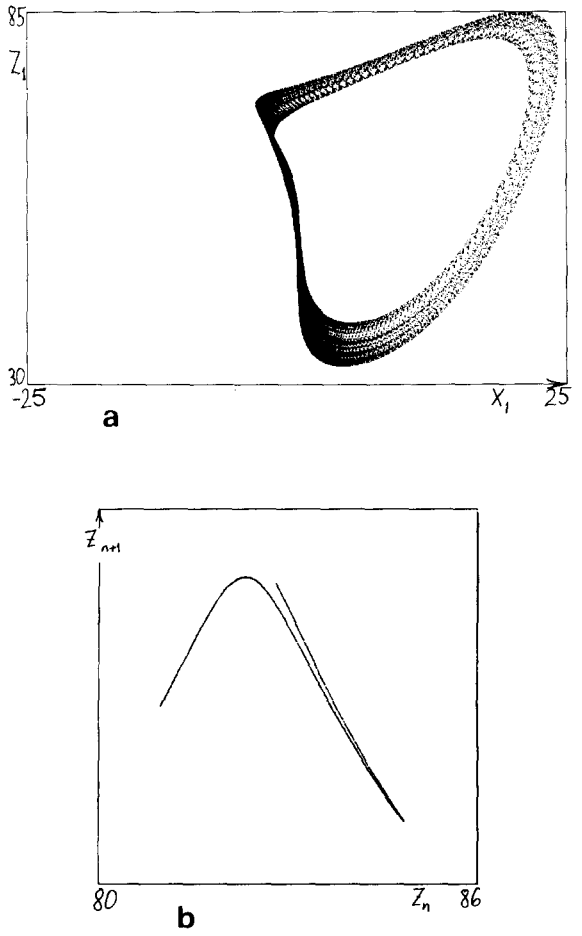

Fig. 9. a) One-sided chaos at $\rho = 58$, $\sigma = 14$, for the $N = 4$ mode system. b) As in fig. 7, Z_{n+1} is plotted versus Z_n, the peaks of $Z_1(t)$; 3800 points are plotted here. Notice the lack of a sharp peak.

system symmetry implies that the reflected orbit (with the fluid moving predominantly in the other direction) must also exist. For fixed σ, as r is increased and enters the "one-sided" region, a one sided periodic orbit appears which period doubles to a one-sided chaotic orbit. At the upper r value of the wedge a crisis occurs with a transition from one-sided to two-sided chaos. Similar behavior is seen in the $N = 1$ system for r large, $b = 1$ and $\sigma = 14$ but these attractors do not coexist with the stable steady state because r_H lies far below this region. It would be interesting to know whether the coexistence of such states with the steady state is experimentally observable in a fluid loop with high Prandtl number.

Our results are all presented in terms of dimensionless variables and parameters. For material parameters appropriate to water at 300 K and with $a = 1$ cm, $R = 50$ cm, the time corresponding to $\Delta\tau = 1$ is approximately 100 s while the temperature difference impressed between the top and center of the tube is approximately $r/4$. If the tube dimensions are changed, the circulation velocity will increase as R/a^2 while the required thermal gradient (W/R) to produce a particular effect increases as $1/a^4$. The steady state solutions in dimensionless variables depend on r but not on σ. For fixed tube dimensions, increasing the fluid's viscosity but not changing its thermal diffusivity will require a larger thermal gradient to achieve the same steady velocity flow pattern and the magnitude of the velocity will not change. If the viscosity is fixed and χ is increased, the flow speed will increase although if r is maintained constant (again by increasing the thermal gradient) the shape of the velocity profile will not change.

4. Discussion

The results reported here are for 1 through 5 Bessel function modes and $r < 100$. Outside the range $6 \leq \sigma \leq 16$ no chaos or even periodic oscillation is found for the five mode case. The transition values of r seem to be converging nicely as N increases except for small $\sigma(\approx 6)$ and for large $\sigma(\approx 16)$. We have argued that the size of the coefficients of the Nth Bessel function mode must go to zero like $N^{-5/2}$. Since we believe we are already seeing this decay as N reaches 5, the behavior seems unlikely to change significantly for more modes. Our solutions that employ either 4 or 5 modes seem to be excellent representations of solutions of the particle differential equation. While these results might be a guide in designing further experiments, it is quite conceivable that the results of those experiments could deviate

significantly from our observations for reasons we discuss below.

It has often been pointed out that the Lorenz system represens too severe a truncation to be expected to actually describe a fluid flow with Bénard boundary conditions. The tube geometry used here physically constrains the fluid and reduces the freedom so that Lorenz type chaotic behavior becomes plausible. We see numerically that increasing the number of modes from one to several decreases the oscillatory tendencies of the solutions. The values of r at which Hopf bifurcations occur more than double. This may heuristically be explained as follows. In the temperature profile of the steady state (fig. 4) we can see the central core temperatures remain nearly constant. It follows that the convective forces accelerate essentially only the outer layer (nearly the wall) while the central core moves because it is dragged viscously. The momentum and drag of the central core appears to inhibit changes in directions of the outer layer.

Will real fluids constrained to such tube exhibit the chaotic oscillations qualitatively like Lorenz's? The experimental studies of Gorman et al. report just such results though we hasten to add that their heating procedures are quite different from ours. In particular they use a constant heat flux on the lower part of the tube. Also, the partial differential equations we use are aimed at the situation where each particle of fluid remains a constant distance from the wall of the tube. For a real fluid there would be some radial motion. In the extreme case the radial motion would mix the fluid to the extent that the temperature at any φ cross section would be nearly constant except for a thin boundary layer at the wall. The derivation of Yorke and Yorke [10] shows that such a turbulent mixing model also satisfies the Lorenz equations. There, unfortunately, the constants in the Lorenz system cannot physically be determined because the actual flow of heat into the fluid depends on the temperature gradient at the wall – that is, on the unknown thickness of the boundary layer. The real situation will be somewhere in between the highly mixed slug flow and our partial differential equation. Since chaotic oscillations of the type described by Lorenz are seen in both cases, we may reasonably expect such oscillations in the real fluid.

References

[1] E.N. Lorenz, Deterministic nonperiodic flow, J. Atmos. Sci. 20 (1963) 130.

[2] J.L. Kaplan and J.A. Yorke, Preturbulence: a regime observed in a fluid flow model of Lorenz, Commun. Math. Phys. 67 (1979) 93.

[3] E. Ott, C. Grebogi and J.A. Yorke, Crises, sudden changes in chaotic attractors and transient chaos, Physica 7D (1983) 181.

[4] J.A. Yorke and E.D. Yorke, Metastable chaos: the transition to sustained chaotic behavior in the Lorenz model, J. Statist. Phys. 21 (1979) 263.

[5] C. Sparrow, The Lorenz Equations: Bifurcations, Chaos and Strange Attractors, (Springer, Berlin, 1982).

[6] P. Welander, On the oscillatory instability of differentially heated fluid loop, J. Fluid. Mech. 29 (1967) 17.

[7] H.F. Creveling, J.F. dePaz, J.Y. Baladi and R.J. Schoenhals, Stability characteristics of a single-phase free convection loop, J. Fluid. Mech. 67 (1975) 65.

[8] M. Gorman, P.J. Widmann and K.A. Robbins, Chaotic flow regimes in a convection loop, Phys. Rev. Lett. 52 (1984) 2241.

[9] A. Mertol and R. Greif, A review of natural circulation loops, in: Natural Convection: Fundamentals and Applications, W. Aung, S. Kakac and R. Viskanta, eds. (Hemisphere P., New York, 1985).

[10] J.A. Yorke and E.D. York, Chaotic Behavior and Fluid Dynamics in Hydrodynamic Instabilities and the Transition to Turbulence, H.L. Swinney and J.P. Gollub, eds. (Springer, Berlin, 1981), pp. 77–95.